The thermal expansion of $(Fe_{1-y}Ni_y)Si$

2017 J. Phys.: Condens. Matter 29 335701

(http://iopscience.iop.org/0953-8984/29/33/335701)

OPEN ACCESS
IOP Publishing
Journal of Physics: Condensed Matter
J. Phys.: Condens. Matter **29** (2017) 335701 (10pp)
https://doi.org/10.1088/1361-648X/aa797d

The thermal expansion of $(Fe_{1-y}Ni_y)Si$

Simon A Hunt, Elizabeth T H Wann, David P Dobson, Lindunka Vočadlo and Ian G Wood

Department of Earth Sciences, University College London, Gower Street, London WC1E 6BT, United Kingdom

E-mail: simon.hunt@ucl.ac.uk

Received 6 April 2017
Accepted for publication 14 June 2017
Published 24 July 2017

Abstract

We have measured the thermal expansion of $(Fe_{1-y}Ni_y)Si$ for $y = 0$, 0.1 and 0.2, between 40 and 1273 K. Above ~700 K the unit-cell volumes of the samples decrease approximately linearly with increasing Ni content. Below ~200 K the unit-cell volume of FeSi falls to a value between that of $(Fe_{0.9}Ni_{0.1})Si$ and $(Fe_{0.8}Ni_{0.2})Si$. We attribute this extra contraction of the FeSi, which is a narrow band-gap semiconductor, to the depopulation of the conduction band at low temperatures; in the two alloys the additional electrons introduced by the substitution of Ni lead to the conduction band always being populated. We have fit the unit-cell volume data with a Debye internal energy model of thermal expansion and an additional volume term, above 800 K, to take account of the volumetric changes associated with changes in the composition of the sample. Using the thermophysical parameters of the fit we have estimated the band gap in FeSi to be 21(1) meV and the unit-cell volume change in FeSi associated with the depopulation of the conduction band to be 0.066(35) $Å^3$/unit-cell.

Keywords: x-ray diffraction, heat capacity, semiconductor, band-gap

(Some figures may appear in colour only in the online journal)

1. Introduction

Iron monosilicide, ε-FeSi, is a member of a class of transition metal monosilicide compounds (including MnSi, FeSi, CoSi, RuSi, ReSi, OsSi) that adopt an unusual B20 type structure (space group $P2_13$, $Z = 4$), in which each species has sevenfold coordination (Pauling and Soldate 1948). The atomic positions in FeSi are slightly removed from the ideal structure, in which the iron and silicon both occupy 4*a* (x, x, x) sites with $x = \pm 0.15451$ (Mattheiss and Hamann 1993, Wood *et al* 1996, Vočadlo *et al* 1999, 2000, 2002). A considerable amount of solid solution is exhibited by $(Fe_{1-y}M_y)(Si_{1-z}N_z)$, where M and N are dopant elements. For example, at ambient pressure the B20 structure is stable with $z_{Al} \lesssim 0.2$ (Delaire *et al* 2013), $y_{Ni} \lesssim 0.6$ (Ackerbauer *et al* 2009, Semenova 2009, Zhang *et al* 2009) and there is complete solid solution between FeSi and many of the other compounds in the class. Nickel monosilicide does not crystallise into the B20 structure at ambient pressure but it adopts the B20 structure above ~10 GPa and 900 K (Lord *et al* 2012, Dobson *et al* 2016).

Natural samples of FeSi, in the form of an aluminium-bearing mineral, naquite, have been found as inclusions in Tibetan hartzburgite rocks (Shi *et al* 2012) and a regolith breccia clast of a lunar highland meteorite (Anand *et al* 2004). Both the naquite and meteoritic samples are nonstoichiometric, being deficient in silicon and containing minor percentage (<2.5 wt.%) impurities. This is consistent with the iron–silicon binary system in which the B20 structure of FeSi is non-stoichiometric (Kubaschewsk 1982). FeSi is a potentially important phase in Earth and planetary sciences because silicon is a potential alloying element in the core of the Earth and other terrestrial planets, as well as being a possible reaction product of silicates and molten iron at the core-mantle boundary (Dubrovinsky *et al* 2003, 2004).

Many of the physical properties of end-member FeSi have unusual temperature dependencies, including the thermal expansion (Mandrus *et al* 1994), heat capacity (Mani *et al* 2008), Seebeck coefficient (Sales *et al* 1994) and magnetic susceptibility (Sales *et al* 1994). The unusual properties are caused by its peculiar electron band structure and FeSi is

Table 1. Ideal and measured chemistry of the three samples.

	Atomic (%)						
	Ideal			Measured			
Sample	Fe	Ni	Si	Fe	Ni	Si	$y = \mathrm{Ni}/(\mathrm{Ni} + \mathrm{Fe})$
FeSi	50		50	50.4(4)		49.6(4)	0
$(Fe_{0.9}Ni_{0.1})Si$	45	5	50	46.3(19)	4.6(18)	49.2(4)	0.10(4)
$(Fe_{0.8}Ni_{0.2})Si$	40	10	50	42.0(30)	8.4(30)	49.6(3)	0.20(7)

commonly described as either a narrow band-gap semiconductor (Delaire *et al* 2011) or a Kondo Insulator (Samuely *et al* 1996, Mani *et al* 2008). Hybridisation between the silicon 3*p* and iron 3*d* bands creates a small gap in the electronic density of states (DOS), which in FeSi (as well as RuSi and OsSi) coincides with the Fermi level (Mattheiss and Hamann 1993, Jarlborg 1997, Sales *et al* 2011). Estimates of the size of the band-gap (E_g) in FeSi range between ~30 and 105 meV from experiments (Schlesinger *et al* 1993, Mandrus *et al* 1994, 1995, Sales *et al* 1994, Park *et al* 1995, Samuely *et al* 1996, Jarlborg 1997, Fäth *et al* 1998, Menzel *et al* 2009) although one indirect estimate is as low as 10 meV (Menzel *et al* 2009). Electronic DOS calculation estimates the band gap to be ~120 meV (Delaire *et al* 2011). The unusual temperature dependencies are not displayed by the other compounds of the class, which are all metals or semi-metals. The low temperature insulating state of $(Fe_{1-y}M_y)(Si_{1-z}N_z)$ is suppressed by substitution of both Fe and Si, which alters the number of *d*-electrons per unit-cell. For Co, Cr and Al, the critical dopant levels to supress the insulator state are $y^{C}_{Co} \sim 0.03$ (Manyala *et al* 2000), $y^{C}_{Cr} \sim 0.02$ (Yadam *et al* 2016) and $z^{C}_{Al} < 0.1$ (Delaire *et al* 2013).

The unit-cell volume of FeSi has been measured between 4 and 1173 K by time of flight neutron diffraction Vočadlo *et al* (2002) and is reported in other studies at non-ambient temperature (Sales *et al* 1994, Delaire *et al* 2013). The thermal expansion of FeSi has been measured by dilatometry by both Krentsis *et al* (1972) and Mandrus *et al* (1994) who also measured the thermal expansion of $Fe_{1-y}Co_ySi$ for $0 \leqslant y \leqslant 0.05$ between 40 and 300 K and showed that the addition of Co to FeSi significantly reduces the thermal expansion and the change is related to the suppression of its semi-conducting properties.

The thermophysical properties of $(Fe_{1-y}Ni_y)Si$ have not previously been studied. Here we use x-ray diffraction to measure the unit-cell volume and thermal expansion of $(Fe_{1-y}Ni_y)Si$, for $0 \leqslant y \leqslant 0.2$, between 40 and 1273 K. The data are analysed using Grüneisen approximations to the zero pressure equation of state, from which the volume change associated with the depopulation of the conduction band and the band-gap of FeSi are estimated.

2. Experiments

Three different samples are studied here with varying levels of nickel; the compositions are nominally: FeSi, $(Fe_{0.9}Ni_{0.1})Si$ and $(Fe_{0.8}Ni_{0.2})Si$. The samples were made by arc-melting high purity iron (>99.97%), silicon (>99.999%) and nickel, at the University of Birmingham. The boules of sample were prepared for x-ray diffraction by grinding to a fine powder under ethanol in an agate pestle and mortar. X-ray diffraction of the samples confirmed the materials adopted the cubic ε-FeSi structure in each case, with no additional phases observed. The chemical composition of the samples was measured by electron probe XRF and is reported in table 1. All samples are deficient in silicon which is normal for this method of making samples. Although the phase diagram of the Fe–Ni–Si ternary indicates that B20 structured (Fe,Ni)Si with >30 at.% Ni is stable at one atmosphere (Ackerbauer *et al* 2009, Zhang *et al* 2009) our attempts to make phase-pure $(Fe_{0.7}Ni_{0.3})Si$ at atmospheric pressure, by arc-melting did not make phase-pure samples. Recent studies have shown that NiSi adopts the B20 structure at high pressure and high temperature (above ~10 GPa and 900 K; Lord *et al* 2012, Wood *et al* 2013, Dobson *et al* 2016); however, our attempted high-pressure (18 GPa) synthesis of $Fe_{0.7}Ni_{0.3}Si$ did not yield a phase-pure sample.

The unit-cell volume as a function of temperature was investigated by x-ray diffraction in a PANalytical X'Pert Pro diffractometer, with Bragg–Brentano parafocusing reflection geometry. The cobalt source is monochromated, by a Ge(1 1 1) Johansson geometry focusing monochromator, to produce a Co $K\alpha_1$ incident beam, the wave-length of which is assumed to be 1.788 996 Å (Hölzer *et al* 1997). The x-ray tube was operated at 40 kV and 30 mA. Variable-width divergence and anti-scatter slits were used, together with a 10 mm wide incident-beam mask, so as to illuminate a 10 × 10 mm area of the sample. Both the incident and diffracted beams had 0.04 radian Soller slits to reduce the axial divergences. The x-ray detector was an 'X'Celerator' position-sensitive detector with an anglular range of $2\theta = \pm 1.061°$ and an effective fixed step size of 0.0167°. Data were collected over the 2θ range from 28 to 155°. Prior to the experiments reported here, the zero 2θ angle of the diffractometer was determined using a Si standard.

Diffraction data between 40 and 300 K were collected using Oxford Cryosystems' PheniX 'Front Loader' low-temperature stage (a modified version of the standard PheniX stage) and between 298 and 1273 K using an Anton Paar HTK1200N heated stage. In both cases the data were collected in 20 K intervals starting at the lowest temperature. In the high-temperature stage, the sample was heated at 5 K min^{-1}, after which it was equilibrated for 6 min (10 min below 373 K) and the data collected in a time of 76 min. The samples were run in air; we initially ran the samples under vacuum but this resulted in significant temperature offsets of

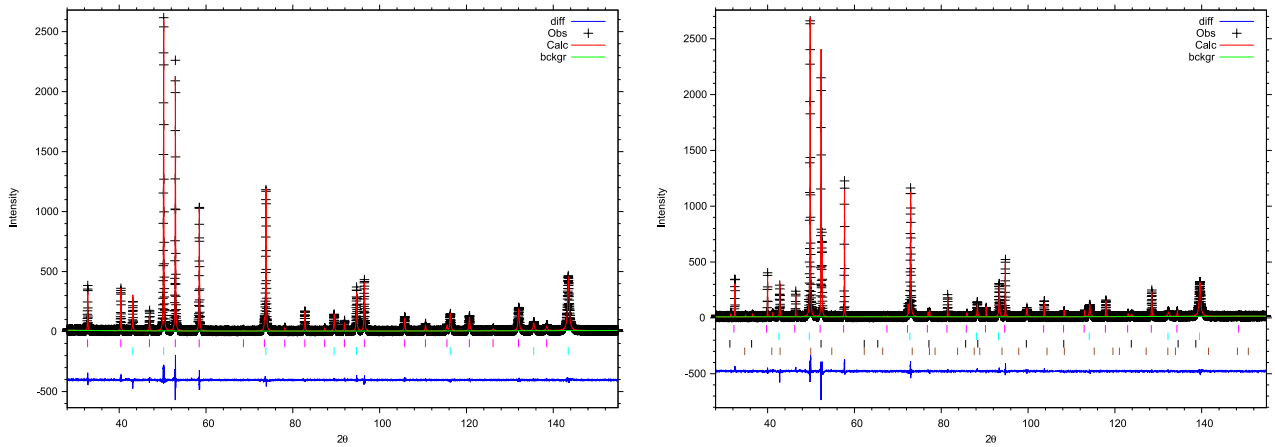

Figure 1. Example x-ray powder diffraction patterns of FeSi at (left) 298 K and (right) 1173 K. Observations (crosses), calculated (red line) and differences (lower trace). The tick markers show the position of the Bragg reflections top down: FeSi, MgO, Fe_3Si, and magnesioferrite.

up to 30 K between the thermocouple and the sample. We have tested the accuracy of the heating stage's thermometry by the melting of high purity gold and measure the melting point to be within 1.5 K of the accepted value (1064 °C). In the PheniX cold stage, the sample was held in an atmosphere of helium exchange gas. The temperature was cooled as quickly as possible (~2 K min^{-1}) to 80 K and then at 1 K min^{-1} to 40 K. After equilibration for 10 min at 40 K the data were collected. Subsequent increases in temperature were at 2 K min^{-1} and the data were collected after a 5–8 min equilibration. The data collections were ~63 min long.

The samples used for the diffraction experiments were mixed with high purity MgO (Aldrich 99.99%) in a ratio of $2(Fe_{1-y}Ni_y)Si$: 3MgO by weight. The MgO was fired overnight at 800 °C in air before mixing. The weight ratio gives approximately the same maximum peak intensity in both the $(Fe_{1-y}Ni_y)Si$ and MgO. The purpose of the MgO was to act as a standard between the three different experiments and confirm that the thermometry is consistent between experiments. When non-cubic materials are examined in this way, the MgO also adds further constraints to the specimen displacements and transparency in the subsequent Rietveld refinements.

The data were analysed by Rietveld refinement in the GSAS suite of programs (Larson and Von Dreele 2000, Toby 2001), after conversion from variable to fixed divergence slit geometry by the diffractometer manufacturer's X'pert HighScorePlus software package. Two phases, MgO and $(Fe_{1-y}Ni_y)Si$, were included in all the refinements. For the nickel bearing phases the site occupancy of the metal site was set to include the nominal percentage Ni and the displacements and thermal vibration of the Fe and Ni were constrained to be the same. The fractional coordinates of the atoms and the atomic displacement parameters were refined along with the unit-cell parameters. As the sample is heated (or cooled) small changes in the position of the sample within the diffractometer take place. This change in position was included in the refinement, as was the sample transparency, and both values were constrained to be the same for all phases. Example diffraction patterns, from FeSi, collected at room temperature and 1173 K are presented in figure 1.

Above ~800 K the apparent weight fraction of MgO in the samples increases. At the same temperature Fe_3Si became detectable in the FeSi diffraction pattern and above ~1000 K Fe_2Si was detectable exolving from the Nickel bearing phases. Above 973 K the FeSi sample reacted with the MgO to produce magnesioferrite ($MgFe_2O_4$) and fayalite (α-Fe_2SiO_4) structured phases; FeSi has a very high affinity for oxygen oxidising even under vacuum at high temperatures (Vočadlo *et al* 2002). There is an apparent loss of silicon in the samples because no silica/silicon rich phases were observed in the diffraction patterns. However, refining the site occupancy for Fe and Si confirms the samples are Si deficient before heating and become more stoichiometric at high temperature as Fe-rich phases are exolved. Due to the additional phases, sequential refinement of the patterns was started at the highest temperature and the additional phases removed from subsequent refinements when their weight percent dropped below 0.01% and/or the unit-cell volume of the additional phases ceased to follow a reasonable volume—temperature relationship.

There is a small offset ($\lesssim$1 in 10^4) in the lattice parameters between the high and low temperature stages. To compensate for this in the subsequent analysis the high temperature data were scaled to match the low temperature volumes. The scaling was done by minimising the residuals of a second order polynomial passing through the 200–393 K data. The scaling factors used for the high temperature data were 0.9999, 0.9998 and 0.9998 for FeSi, $(Fe_{0.9}Ni_{0.1})Si$ and $(Fe_{0.8}Ni_{0.2})Si$ respectively. The scaling has minimal effect on the fitted parameters in equation (7), below; with and without scaling the data, these were within two standard deviations of each other.

3. Results

The unit-cell volumes of the (Fe,Ni)Si samples, returned by the Rietveld refinement, are plotted in figure 2 and listed in table 2. Table 2 also lists the additional phases included in each refinement. Between ~100 and 250 K, the unit-cell volumes of FeSi measured here are almost indistinguishable from those previously published by Vočadlo *et al* (2002), whilst at high temperatures the unit-cell volumes of Vočadlo *et al*

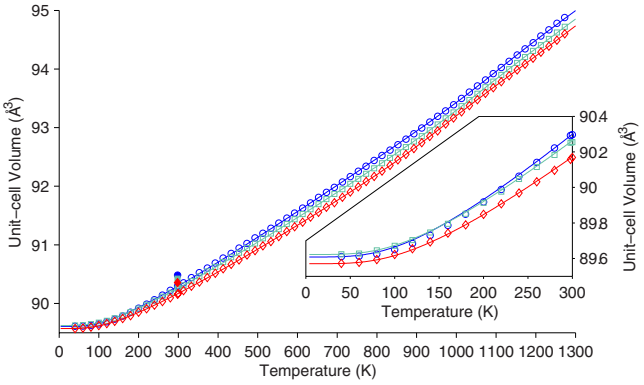

Figure 2. Measured unit-cell volumes of $Fe_{1-y}Ni_ySi$ against temperature. FeSi—circles, $Fe_{0.9}Ni_{0.1}Si$—squares, $Fe_{0.8}Ni_{0.2}Si$—diamonds. Open symbols are the data, filled symbols are the recovered sample after high temperature measurements and the lines are fits of equation (7) to the data. Unit-cell volume error bars are omitted because errors are smaller than the symbols. The inset is an enlargement of the data below 300 K.

(2002) become systematically smaller than those measured here; at 1100 K the difference is 0.14% (figure 3).

Overall, the difference in unit-cell volume between the FeSi and the Nickel bearing phases (figure 3) is small compared to the changes in unit-cell volume with temperature (figure 2). At temperatures greater than ~700 K when the conduction band of the FeSi semiconductor is populated by electrons, the substitution of nickel into FeSi causes a decrease in unit-cell volume and a corresponding increase in density. The decrease in unit-cell volume and increase in density are approximately linear with Ni content and temperature independent. At low temperature, however, the effect of nickel on FeSi is very different. Below 200 K, FeSi has a smaller unit-cell volume than $Fe_{0.9}Ni_{0.1}Si$ but not $Fe_{0.8}Ni_{0.2}Si$. For $0 < y \lesssim 0.1$, the substitution of Ni into $(Fe_{1-y}Ni_y)Si$ places electrons in the conduction band and increases the unit-cell volume, at higher Ni concentrations ($y \gtrsim 0.1$) increasing the nickel concentration results in a unit-cell volume contraction. The nickel-bearing samples ($y = 0.1$ and 0.2) here are probably metallic because their Ni content is greater than y^C for either cobalt or chromium and the differences in their behaviour is minimal.

3.1. Volume-temperature models

To quantify the effect of doping FeSi with nickel both empirical and theoretical models of volumetric thermal expansion have been fitted to the data. For high temperature data (>~300 K) an empirical form of the thermal expansion is commonly used (Fei 1995). In this formulation the unit-cell volume is given by:

$$V(T) = V_{T_0} \exp\left[\int_{T_0}^{T} \alpha(T)\mathrm{d}T\right] \tag{1}$$

where V_{T_0} is the volume at the reference temperature T_0 (here taken to be 300 K) and $\alpha(T)$ is the volumetric thermal expansion coefficient with the 1st order form:

$$\alpha(T) = \alpha_0 + \alpha_1 T \tag{2}$$

The values of V_{T_0}, α_0 and α_1, fitted to our data between 300 and 1273 K, are shown in table 3.

One theoretical approach to the unit-cell volume and thermal expansion, that fits the data at all temperatures, is to use Debye and Grüneisen approximations to make a zero pressure equation of state (Wallace 1998). This model in which the effects of thermal expansion are considered equivalent to elastic strain also allows the Debye temperature to be estimated. A second order Grüneisen approximation is appropriate for data covering a wide temperature range (Vočadlo *et al* 2002, Lindsay-Scott *et al* 2007) taking the form:

$$V(T) = V_0 + \frac{V_0 U}{Q - bU} \tag{3}$$

where

$$Q = V_0 K_0/\gamma \tag{4}$$

and

$$b = (K' - 1)/2. \tag{5}$$

V_0 is the unit-cell volume at $T = 0$ K, K_0 and K' are the bulk modulus and its first derivative with respect to pressure respectively and γ is a Grüneisen parameter, which is assumed to be constant. The internal energy, U, as a function of temperature is calculated using the Debye approximation (Poirier 2000):

$$U(T) = 9Nk_BT\left(\frac{T}{\theta_D}\right)^3 \int_0^{\theta_D/T}\left(\frac{x^3}{\exp(x) - 1}\right)\mathrm{d}x. \tag{6}$$

In equation (6), k_B is Bolzmann's constant, θ_D is the Debye temperature and N is the number of atoms in the unit-cell. For the phases studied here $N = 8$.

Whilst equation (3) provides a reasonably good fit to the data, the residuals remain significant and are systematic with temperature and between the samples. The systematics in the residuals are unlikely to be due to errors in the thermometry because: (1) the melting of gold was measured at its accepted melting temperature, (2) the residuals for the (Fe,Ni)Si phases are weakly anti-correlated with same fit of equation (3) to the MgO unit-cell volumes and (3) the residuals between the FeSi data obtained by neutron diffraction (Vočadlo *et al* 2002), and the fit to equation (3) are identical to those of this study. The systematic residuals are therefore likely to be due to changes in the samples at high temperature. Above 800 K additional diffraction peaks appear in the patterns, increasing in intensity with time and temperature, and the unit-cell volumes of samples recovered to ambient temperature after the high-temperature measurements are significantly larger than the initial volumes (figures 2 and 3). This type of behaviour is similar to that observed in the magnetic susceptibility of FeSi (Jaccarino *et al* 1967); above ~760 K, the magnetic susceptibility deviates from the lower temperature relationship and does not return to it when the temperature is lowered. To account for the sample changes during heating a modified version of equation (3) was used:

$$V(T) = V_0 + \frac{V_0 U}{Q - bU} + h\left[\mathrm{erf}\left(\frac{T - T_{\mathrm{cent}}}{w}\right) + 1\right], \tag{7}$$

Table 2. The unit-cell volumes of $Fe_{1-y}Ni_ySi$ measured in this study. The listed values are unscaled and the numbers in parenthesis are one standard error of the least significant digit.

Temperature (K)	Unit-cell volume (Å³)		
	FeSi	$(Fe_{0.9}Ni_{0.1})Si$	$(Fe_{0.8}Ni_{0.2})Si$
Low temperature stage			
40	89.6106(15)	89.6245(15)	89.5723(11)
60	89.6137(15)	89.6279(13)	89.5781(14)
80	89.6251(15)	89.6461(13)	89.5941(14)
100	89.6500(15)	89.6712(14)	89.6226(8)
120	89.6850(15)	89.7036(14)	89.6549(13)
140	89.7300(15)	89.7466(13)	89.6936(14)
160	89.7865(15)	89.7954(13)	89.7425(14)
180	89.8486(7)	89.8520(13)	89.7897(14)
200	89.9181(15)	89.9135(14)	89.8487(14)
220	89.9880(15)	89.9763(14)	89.9078(15)
240	90.0624(15)	90.0474(14)	89.9691(15)
260	90.1413(15)	90.1153(14)	90.0315(14)
280	90.2221(15)	90.1829(14)	90.0964(14)
300	90.2971(15)	90.2550(14)	90.1682(8)
High temperature stage			
298	90.3015(13)	90.2697(13)	90.1754(14)
313	90.3601(13)	90.3258(13)	90.2349(14)
333	90.4488(13)	90.3998(13)	90.3099(14)
353	90.5314(13)	90.4797(13)	90.3813(14)
373	90.6132(13)	90.5647(13)	90.4600(14)
393	90.6979(13)	90.6402(13)	90.5322(14)
413	90.7845(13)	90.7242(13)	90.6104(14)
433	90.8623(13)	90.8053(13)	90.6849(14)
453	90.9524(13)	90.8822(13)	90.7604(14)
473	91.0322(13)	90.9631(13)	90.8429(14)
493	91.1252(13)	91.0405(13)	90.9187(14)
513	91.2059(13)	91.1277(14)	91.0007(15)
533	91.2893(13)	91.2096(14)	91.0732(15)
553	91.3792(13)	91.2854(14)	91.1574(15)
573	91.4634(13)	91.3719(14)	91.2441(15)
593	91.5521(13)	91.4543(14)	91.3271(15)
613	91.6373(13)	91.5417(13)	91.4041(16)
633	91.7238(13)	91.6242(14)	91.4900(15)
653	91.8176(13)	91.7115(14)	91.5718(16)
673	91.9016(13)	91.7978(14)	91.6579(16)
693	91.9920(13)	91.8856(14)	91.7354(16)
713	92.0813(13)[a]	91.9661(15)	91.8301(17)
733	92.1740(13)[a]	92.0587(15)	91.9186(17)
753	92.2659(13)[a]	92.1446(14)	92.0069(16)
773	92.3523(13)[a]	92.2306(15)	92.0988(16)
793	92.4465(13)[a]	92.3232(15)	92.1859(16)
813	92.5351(13)[a]	92.4096(15)	92.2760(16)
833	92.6239(13)[a]	92.5015(14)	92.3729(15)
853	92.7168(13)[a]	92.5945(14)	92.4680(16)
873	92.8133(13)[a]	92.6870(14)	92.5614(16)
893	92.9044(13)[a]	92.7807(14)	92.6605(16)
913	93.0028(12)[a]	92.8727(13)	92.7604(16)
933	93.1015(13)[a]	92.9732(14)	92.8677(16)
953	93.2029(13)[a]	93.0727(6)	92.9613(16)
973	93.2956(13)[a]	93.1775(6)	93.0804(6)
993	93.4008(13)[a]	93.2787(6)[d]	93.1832(7)[d]
1013	93.5074(13)[b]	93.3849(6)[d]	93.2869(7)[d]

(*Continued*)

Table 2. (*Continued*)

Temperature (K)	Unit-cell volume (Å³)		
	FeSi	$(Fe_{0.9}Ni_{0.1})Si$	$(Fe_{0.8}Ni_{0.2})Si$
1033	93.6166(13)[b]	93.4888(5)[d]	93.3934(17)[d]
1053	93.7204(13)[b]	93.5973(6)[d]	93.4935(17)[d]
1073	93.8223(13)[b]	93.7078(6)[d]	93.6024(17)[d]
1093	93.9312(13)[b]	93.8047(6)[d]	93.7002(17)[d]
1113	94.0350(13)[b]	93.9174(6)[d]	93.8016(6)[d]
1133	94.1407(13)[b]	94.0145(6)[d]	93.9050(6)[d]
1153	94.2477(13)[b]	94.1230(6)[d]	94.0009(17)[d]
1173	94.3520(13)[b]	94.2230(6)[d]	94.0998(17)[d]
1193	94.4570(13)[b]	94.3285(15)[d]	94.2025(17)[d]
1213	94.5737(14)[c]	94.4245(15)[d]	94.3039(17)[d]
1233	94.6755(15)[c]	94.5330(16)[d]	94.4076(6)[d]
1253	94.7876(14)[c]	94.6418(6)[d]	94.5092(6)[d]
1273	94.8875(15)[c]	94.7396(6)[d]	94.6181(7)[d]

Note. The letters after the volumes indicate which additional phases were included in the refinements:
[a] Fe_3Si,
[b] $Fe_3Si + MgFe_2O_4$,
[c] $Fe_3Si + MgFe_2O_4$ + fayalite and
[d] $(Fe_{1-y}Ni_y)_2Si$.

where the additional term is an error function with height $2h$, width w and centred on T_{cent}. Equation (7) was fitted to the unit-cell volume data by non-linear weighted least squares. The data were weighted by the standard error of the unit-cell volume, except for the data at 40 K on which there is an additional 1000 fold weighting which compensates for the lack of data below 40 K where thermal expansion is known to be minimal (Vočadlo *et al* 2002). Without the additional weighting the biggest residuals between the data and the fitted model are at 40 K and V_0 is very different from the 40 K datum. The additional weighting was decided upon by trial and error. The free fit of equation (7) to the FeSi and $Fe_{0.9}Ni_{0.1}Si$ data sets is underconstrained because the error function term overlaps with the end of the data set. Therefore, h and w were constrained to be the same as those for $(Fe_{0.8}Ni_{0.2})Si$.

The solid lines in figures 2 and 3 are the result obtained from fitting equation (7) to the volume—temperature data; the thermophysical values are listed in table 3. Equation (7) is a very good fit to the data with no systematic differences between the data and the fit for the $(Fe_{0.8}Ni_{0.2})Si$ data. The residuals between the fit and the FeSi data on the other hand are systematic (figure 3). The systematic residuals indicate that equation(7) does not provide a comprehensive description of the thermal expansion behaviour of FeSi.

The pressure derivative of the bulk modulus, K', can be obtained directly from the coefficient b (equation (5)). The resulting value for FeSi, $K' = 3.5(2)$ is within error of previously published values for K', which range between 3.5(4) (Knittle and Williams 1995) and 6.6(20) (Whitaker *et al* 2009). The K' values for the Ni-bearing phases (table 3) increase with nickel content (y) but remain reasonable. The Debye temperature for FeSi measured here, 477(7) K, lies within the range of previous estimates, which range from <337 K (Paschen *et al* 1997) to >680 K (Petrova *et al* 2011). The Debye temperature increases nonlinearly with nickel content. Indeed all the freely

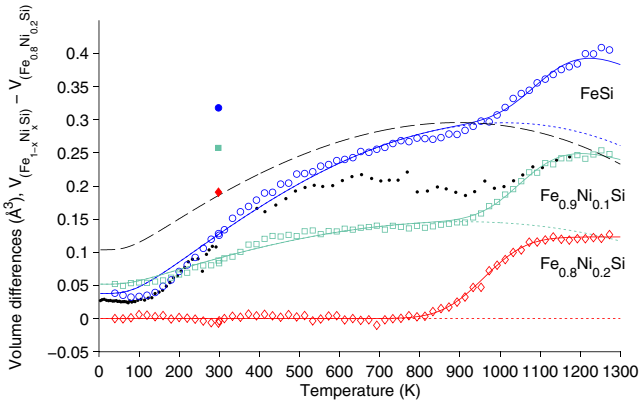

Figure 3. Volume differences from the $Fe_{0.8}Ni_{.2}Si$ data's Debye component of equation (7). FeSi—circles, $Fe_{0.9}Ni_{0.1}Si$—squares, $Fe_{0.8}Ni_{0.2}Si$—diamonds. The open symbols are the data, the filled symbols are the recovered sample after high temperature measurements. The solid lines are fits of equation (7) and the the dashed lines are volumes of the Debye component (equation (3)). The black dots are the data of Vočadlo *et al* (2002). The long dashed line is the volume difference of the putative metallic FeSi phase (see text for details). Unit-cell volume error bars are omitted because errors are smaller than the symbols.

Table 3. Thermoelastic properties of the samples; the numbers in parenthesis are one standard error of the least significant digit. The Grüneisen parameter (γ) is calculated assuming $K_0 = 176(3)$ GPa. #—the values were fixed in the fitting, see text for details.

Parameter	FeSi	$(Fe_{0.9}Ni_{0.1})Si$	$(Fe_{0.8}Ni_{0.2})Si$
Polynomial model (equation (3), between 300 and 1273 K)			
V_{T300} (Å^3)	90.328(4)	90.286(6)	90.171(7)
α_0 (K^{-1})	$3.88(4) \times 10^{-5}$	$3.56(5) \times 10^{-5}$	$3.56(5) \times 10^{-5}$
α_1 (K^{-2})	$1.51(5) \times 10^{-8}$	$1.80(6) \times 10^{-8}$	$1.76(7) \times 10^{-8}$
Modified Debye model (equation (7))			
Q (J)	$6.84(4) \times 10^{-18}$	$7.39(3) \times 10^{-18}$	$7.75(3) \times 10^{-18}$
b	1.27(10)	2.22(7)	3.06(8)
θ_D (K)	478(6)	482(5)	496(3)
V_0 (Å^3)	89.6086(4)	89.6226(3)	89.5708(1)
h (Å^3)	6.2×10^{-2} #	6.2×10^{-2} #	$6.2(4) \times 10^{-2}$
w (K)	118 #	118 #	118(11)
T_{cent} (K)	1095(12)	1051(4)	960(4)
Derived values			
K'	3.5(2)	5.6(1)	7.1(2)
γ	2.30(4)	2.13(4)	2.03(4)

varying parameters either increase or decrease with Ni content apart from V_0.

A bulk modulus is required to derive the Grüneisen parameter (γ) from the experimental data (equation (4)). The measured values for the bulk modulus of FeSi range between ~114 GPa (Zinoveva *et al* 1974) and 221.7(32) GPa (Sata *et al* 2010), giving values of γ for FeSi between 1.49(1) and 2.90(5). The median value of the published bulk modulus, excluding the extreme values, is 176(3) GPa (Ross 1996), which we take to be the bulk modulus for FeSi. The bulk modulus of the Ni bearing phases has not been measured we therefore to

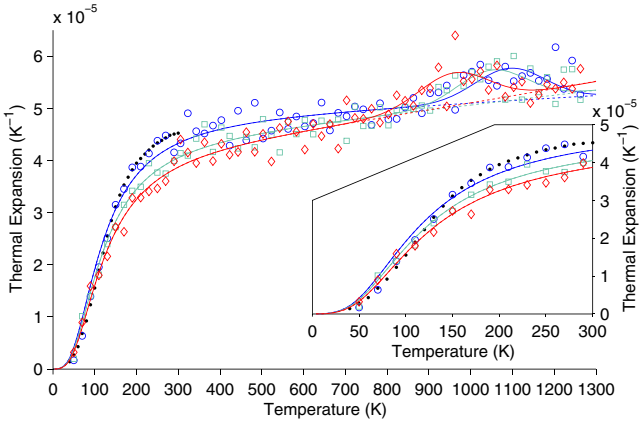

Figure 4. Thermal expansion of phases; FeSi—circles, $Fe_{0.9}Ni_{0.1}Si$—squares, $Fe_{0.8}Ni_{0.2}Si$—diamonds. The symbols are instantaneous thermal expansion calculated from the data, the solid lines are the thermal expansion derived from the equation (5) and the dashed lines are from equation (3). The black dots are the experimental data of Mandrus *et al* (1994) for FeSi.

calculate their Grüneisen parameters we assume K_0 to be the same for all samples and equal to the bulk modulus of FeSi. For FeSi we get $\gamma = 2.30(4)$.

The centroid of the error function term decreases in temperature with increasing nickel content. The temperatures at which its effect first becomes significant are not coincident with the start of exsolution of the additional phases. The exsolution starts at a lower temperature in FeSi and higher temperatures in the Ni-bearing samples. It would therefore appear to be a phenomenon independent of the exsolution. The physical cause of the step in unit-cell volume is unclear: Jaccarino *et al* (1967) attributed changes in their magnetic susceptibility-temperature relationship at ~760 K to 'the ideal FeSi structure becoming disordered' but previously reported structural parameters of FeSi (Vočadlo *et al* 2002) do not show any significant change in behaviour at these temperatures. Some other metals and ceramics show superficially similar steps in their volumes with temperature caused by the demise of magnetic constrictions (Nix and MacNair 1941) and a superionic transition (Cooper *et al* 2014).

3.2. Thermal expansion

The quality of fit between the model and the FeSi data is also reflected in the thermal expansion. Figure 4 shows the volumetric thermal expansion of the $(Fe_{1-y}Ni_y)Si$ samples obtained from:

$$\alpha(\overline{T}) = \left(\frac{1}{V(\overline{T})}\right)\left(\frac{dV}{dT}\right). \quad (8)$$

Where $\overline{T}$ is the mean temperature of two adjacent measurements and dV/dT is the point-to-point volume change. The solid lines in figure 4 are the thermal expansions from differentiation of equation (7). The error function in equation (7) manifests in the thermal expansion as the Gaussian peaks centered around 1000 K. The correspondence between the

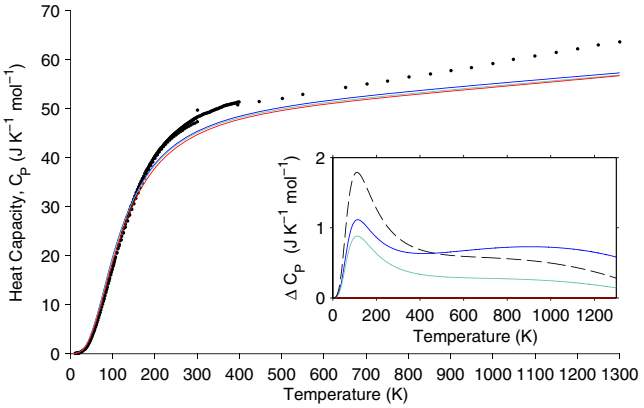

Figure 5. Calculated C_P for the samples; FeSi—blue, $Fe_{0.9}Ni_{0.1}Si$—green, $Fe_{0.8}Ni_{0.2}Si$—red, black symbols are experimental measurements of the heat capacity of FeSi (Krentsis *et al* 1963, Acker *et al* 1999, Mani *et al* 2008). Inset: difference in heat capacities from the $Fe_{0.8}Ni_{0.2}Si$ phase derived from equation (10), the long-dashed line is C_P of the putative metallic-FeSi phase.

data and model is good but for the FeSi the thermal expansions predicted by the fit are too high at ~100 K and too low at ~300 K. Our experimental data are in excellent agreement with previous dilatometry measurements (Mandrus *et al* 1994). As expected from the volume data, the thermal expansion of FeSi is greater than that of the Ni doped phases at low temperatures and the thermal expansions converge at high temperatures. The thermal expansion of the Debye component of the model (figure 4, dashed lines) is the same for all the phases at ~1000 K.

The thermal expansion from the polynomial fits (equation (1)) were calculated for the samples between 300 and 1273 K. Using all the elevated-temperature data for this is reasonable because the step in volume around 1000 K is real. There is very good agreement between the polynomial thermal expansions and the thermal expansion from equation (7). The thermal expansion is the same for both Ni-bearing phases, both of which are smaller than the FeSi thermal expansion at 300 K and increase faster with temperature.

3.3. Heat capacity

The volumetric or isochoric heat capacity (C_V) is the change in internal energy with temperature, at constant volume (Poirier 2000):

$$C_V = \left(\frac{\partial U}{\partial T}\right)_V. \tag{9}$$

The assumption of the Debye model for internal energy (equation (6)), therefore gives:

$$C_V = 9nN_A k_B \left(\frac{T}{\theta_D}\right)^3 \int_0^{\theta_D/T} \left(\frac{x^4 \exp(x)}{(\exp(x)-1)^2}\right) dx. \tag{10}$$

Where n is the number of atoms per formula unit and N_A Avogadro's number. Experimental measurements of heat capacity are made at constant pressure and the isobaric heat capacity (C_P) is related to the isochoric heat capacity by:

$$\left(\frac{C_P}{C_V}\right) = 1 + \gamma^{th}\alpha T. \tag{11}$$

For our data, the thermal expansion (α), Debye temperature (θ_D) and C_V are obtained directly from the fit of equation (7) to the data. We assume the Grüneisen parameter in equation (4) (γ) and the thermal Grüneisen parameter (γ^{th}) to be the same.

The derived values of C_P for our data are plotted in figure 5, together with the experimental results for FeSi. The estimate of C_P for FeSi agrees well with the measurements until ~200 K, above which our estimates significantly underestimate the heat capacity. At 1297 K the underestimate of C_P is ~7% and even using the maximum value for γ we do not match the experimental heat capacity values.

3.4. Electronic band gap of FeSi

In general the heat capacity of a system is (Gopal 1966, Mani *et al* 2008):

$$C = C_{el} + C_{ph} + C_{mag} + C_{Sch} \tag{12}$$

where C_{el}, C_{ph} and C_{mag} are the electron, phonon and magnetic contributions to the heat capacity respectively. The Schottky contribution to the heat capacity (C_{Sch}) arises from the semiconductor band-gap (E_g) (Aronzon *et al* 1993). When $T \ll E_g/k_B$ only the lower energy level of the band gap is occupied whilst when $T \gg E_g/k_B$ the two levels are almost equally occupied. At intermediate temperatures there is a peak in C_{Sch} arising from variable occupancy of the energy levels. This contribution to the heat capacity (C_{Sch}) is expected to be of the form:

$$C_{sch} = ck_B \left(\frac{E_g}{k_B T}\right)^2 \left(\frac{g_0}{g_1}\right) \frac{\exp(E_g/k_B T)}{(1 + (g_0/g_1)\exp(E_g/k_B T))^2}. \tag{13}$$

Where g_0 and g_1 are the degeneracies of the levels above and below the band-gap and c is the number of carriers.

The band-gap in the electron structure is always present in the B20 FeSi structure type and therefore there is always Schottky contribution to the heat capacity. For metallic samples ($y > y^C$ and, in FeSi itself, $T \gg E_g/k_B$) the contribution of C_{Sch} to the internal energy is always present and close to its maximum value. It is only at low temperatures when $y < y^C$ that C_{Sch} contributes less than its maximum value to the internal energy.

Assuming that above (y^C) the thermoelastic parameters (Q, V_0, b and θ_D—generically [Π]—equations (3) and (7)) vary linearly with y:

$$[\Pi]_X = [\Pi]_0 + \frac{d[\Pi]}{dy} y \tag{14}$$

where d[Π]/dy is the change of thermoelastic parameter with Ni concentration (y) and $[\Pi]_0$ is the set of thermoelastic parameters for $y = 0$ which include the metallic, maximum contribution of C_{sch} to the internal energy. The set of parameters $[\Pi]_0$ is therefore the thermophysical properties of a hypothetical metallic-FeSi phase. The values of $[\Pi]_0$ and

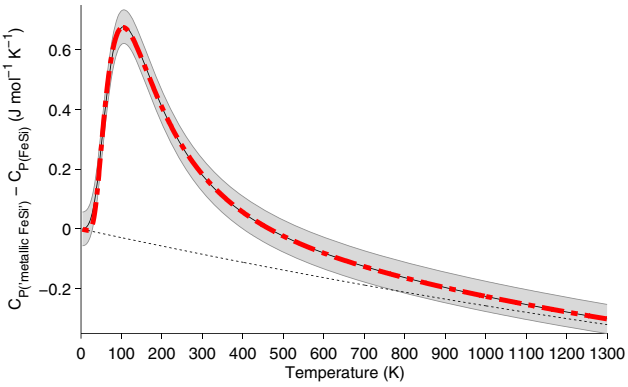

Figure 6. The difference in C_P between 'metallic-FeSi' and observed FeSi. The dashed black line is the linear background and the red line is C_{Sch} calculated as described in the text.

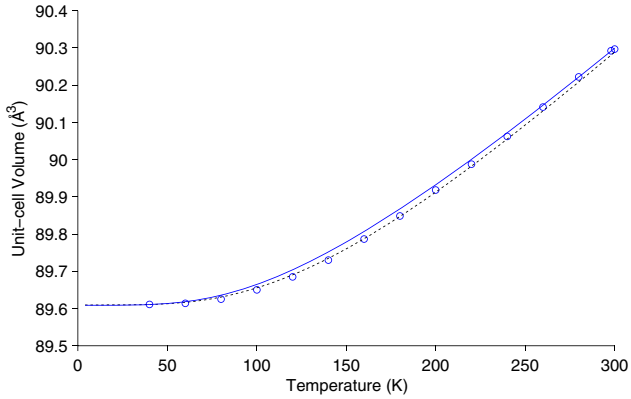

Figure 7. Unit-cell volumes of FeSi below 300 K (circles); the lines are fits of equation (7) to the data with a Debye internal energy (equation (6), blue solid line) and the integral over the heat capacity (equation (9), black dashed line). Unit-cell volume error bars are omitted because errors are smaller than the symbols.

d[Π]/dy have been calculated from the values in tables 2 and 3 for $(Fe_{0.9}Ni_{0.1})$ Si and $(Fe_{0.8}Ni_{0.2})$Si which are assumed to have $y > y^C$. The values for [Π]0 are found to be: $V_0 = 89.675(35)$ Å^3, $Q = 7.03(24) \times 10^{-18}$ J, $b = 1.39(56)$ and $\theta_D = 468(10)$ K. From this, the unit-cell volume and heat capacity of the hypothetical metallic-FeSi have been calculated; these are plotted as dashed lines in figure 3 and the inset of figure 5 respectively.

The unit-cell volumes of the hypothetical and real FeSi phases are similar at high temperatures, as should be expected because in both phases the conduction band is populated at high temperature. This validates the assumption of linearity in equation (14). At low temperatures, the unit-cell volume of the 'metallic-FeSi' is always greater than that of $(Fe_{0.9}Ni_{0.1})$ Si. At 0 K the 'metallic-FeSi' has a unit-cell volume 0.066(35) Å^3 larger than the real FeSi; this volume is associated with the population of the conduction band in FeSi and corresponds to a density decrease of 0.07%. The change in volume is approximately half that of the step at high temperature.

The difference in C_P between the 'metallic-FeSi' and measured FeSi is C_{Sch} (figure 6). Fitting equation (13) plus a linear background to this difference predicts $E_g = 21(1)$ meV, $N = 5(^{+3}_{-2}) \times 10^{11}$ electrons mol^{-1} and $g_0/g_1 = 1.7(^{+13}_{-5})$. The value for E_g estimated here is low compared to previous values which range from ~30 to 105 meV. However, the fit of equation (7) to the FeSi data (figure 3) has systematic residuals because the internal energy formulation (equation (6)) is not correct for a semi-conductor because it does not include the Schottky contribution to the heat capacity. The Schottky contribution to the heat capacity has to be present in the experimentally measured heat capacity. The fit of equation (7), with the integral over the isochoric heat capacity (equations (9) and (11)) as the internal energy, better matches the FeSi data below 300 K and is indistinguishable to the fit with a Debye internal energy (equation (6)) above 300 K (figure 7). We do not report a model with an internal energy model that accounts for the Schottky contribution properly because the fit is severely underconstrained.

4. Conclusions

We have measured the thermal expansion of Ni free and Ni-doped FeSi between 40 and 1273 K. Above ~700 K the decrease in unit-cell volume with Ni content is approximately linear. The commensurate increase in density is small; the difference in density between FeSi and $(Fe_{0.8}Ni_{0.2})$Si at 1273 K is ~0.97%. This suggests that the effect of nickel on the density of iron–silicon alloys is negligible at core conditions for the terrestrial planets.

The unit-cell volumes as a function of temperature are well described by a Debye internal energy model with an additional volume term at high temperature. By assuming a linear change in material properties in the Ni-bearing phases we have calculated the thermophysical properties of a hypothetical FeSi-metal which we predict would have a value of V_0 that is 0.066(35) Å^3 greater than that of the real material. We have used this model to estimate the band gap in FeSi to be 21(1) meV, in reasonable agreement, although somewhat lower than previous estimates of E_g which range between 30 and 120 meV.

Acknowledgments

SAH was funded by a NERC post-doctoral research fellowship (NE/H016309/1); DPD, LV and SAH were funded by NERC standard grants NE/H003975/1 and NE/L006898/1. The samples were synthesised by Dr Seyed Koophayeh in the Materials and Metallurgy department of the University of Birmingham.

ORCID

Simon A Hunt https://orcid.org/0000-0003-3817-8835
David P Dobson https://orcid.org/0000-0002-0890-0121
Lindunka Vočadlo https://orcid.org/0000-0002-2577-0277
Ian G Wood https://orcid.org/0000-0001-9555-6658

References

Acker J, Bohmhammel K, van den Berg G J K, van Miltenburg J C and Kloc C 1999 Thermodynamic properties of iron silicides FeSi and α-$FeSi_2$ *J. Chem. Thermodyn.* **31** 1523–36
Ackerbauer S, Krendelsberger N, Weitzer F, Hiebl K and Schuster J C 2009 Intermetallics the constitution of the ternary system Fe–Ni–Si *Intermetallics* **17** 414–20

Anand M, Taylor L A, Nazarov M A, Shu J, Mao H-K and Hemley R J 2004 Space weathering on airless planetary bodies: clues from the lunar mineral hapkeite *Proc. Natl Acad. Sci. USA* **101** 6847–51

Aronzon B A, Galeczki G and Nimtz G 1993 The electronic specific heat of narrow-gap semiconductors *Phil. Mag.* B **67** 847–54

Cooper M W D, Murphy S T, Fossati P C M, Rushton M J D and Grimes R W 2014 Thermophysical and anion diffusion properties of $(U_x,Th_{1-x})O_2$ *Proc. R. Soc.* A **470** 20140427

Delaire O, Al-Qasir I I, Ma J, dos Santos A M, Sales B C, Mauger L, Stone M B, Abernathy D L, Xiao Y and Somayazulu M 2013 Effects of temperature and pressure on phonons in $FeSi_{1-x}Al_x$ *Phys. Rev.* B **87** 184304

Delaire O, Marty K, Stone M B, Kent P R C, Lucas M S, Abernathy D L, Mandrus D and Sales B C 2011 Phonon softening and metallization of a narrow-gap semiconductor by thermal disorder *Proc. Natl Acad. Sci. USA* **108** 4725–30

Dobson D P *et al* 2016 The phase diagram of NiSi under the conditions of small planetary interiors *Phys. Earth Planet. Inter.* **261** 196–206

Dubrovinsky L *et al* 2003 Iron–silica interaction at extreme conditions and the electrically conducting layer at the base of Earth's mantle *Nature* **422** 58–61

Dubrovinsky L, Dubrovinskaia N, Langenhorst F, Dobson D, Rubie D, Geßmann C, Le Bihan T and Crichton W A 2004 Reaction of iron and silica at core-mantle boundary conditions *Phys. Earth Planet. Inter.* **146** 243–7

Fäth M, Aarts J, Menovsky A A, Nieuwenhuys G J and Mydosh J A 1998 Tunneling spectroscopy on the correlation effects in FeSi *Phys. Rev.* B **58** 15483–90

Fei Y 1995 *Thermal Expansion - Mineral Physics & Crystallography: A Handbook of Physical Constants* ed T J Ahrens (Washington, DC: American Geophysical Union) (https://doi.org/10.1029/RF002p0029)

Gopal E S R 1966 *Specific Heats at Low Temperatures* (Berlin: Springer) (https://doi.org/10.1007/978-1-4684-9081-7)

Hölzer G, Fritsch M, Deutsch M, Härtwig J and Förster E 1997 Ka1,2 and Kb1,3 x-ray emission lines of the 3*d* transition metals *Phys. Rev.* A **56** 4554–68

Jaccarino V, Wertheim G K, Wernick J H, Walker L R and Arajs S 1967 Paramagnetic excited state of FeSi *Phys. Rev.* **160** 476–82

Jarlborg T 1997 ϵ-FeSi: a material sensitive to thermal disorder *Phys. Lett.* A **236** 143–7

Knittle E and Williams Q 1995 Static compression of ε-FeSi and an evaluation of reduced silicon as a deep Earth constituent *Geophys. Res. Lett.* **22** 445–8

Krentsis R P, Gel'd P V and Kalishevich G I 1963 Thermochemistry of iron silicides. Heat capacity, enthalpy, and entropy of iron silicides *Izv. Vyss. Uchebn. Zaved. Chernaya Met* **6** 161–8

Krentsis R P, Kalishevich G I, Gel'd P V and Andreeva L P 1972 Thermal expansion of monosilicides of chromium, manganese, iron and cobalt *Soviet Phys. J.* **15** 143

Kubaschewsk O 1982 Iron–silicon *Iron-Binary Phase Diagrams* (Berlin: Springer) pp 136–9

Larson A C and Von Dreele R B 2000 *General Structure Analysis System (GSAS)* Los Alamos National Laboratory Report LAUR 86–748

Lindsay-Scott A, Wood I G and Dobson D P 2007 Thermal expansion of $CaIrO_3$ determined by x-ray powder diffraction *Phys. Earth Planet. Inter.* **162** 140–8

Lord O T, Vočadlo L, Wood I G, Dobson D P, Clark S M and Walter M J 2012 High-pressure phase transitions and equations of state in NiSi. II. Experimental results *J. Appl. Crystallogr.* **45** 726–37

Mandrus D, Sarrao J L, Migliori A, Thompson J D and Fisk Z 1995 Thermodynamics of FeSi *Phys. Rev.* B **51** 4763–7

Mandrus D, Sarrao J L, Thompson J D, Hundley M F, Migliori A and Fisk Z 1994 Thermal expansion study of $Fe_{1-x}Co_xSi$ *Physica* B **199 & 200** 471–2

Mani A, Janaki J, Sen S, Bharathi A and Hariharan Y 2008 Specific heat studies on Ru substituted FeSi Kondo insulator *Solid State Commun.* **146** 391–4

Manyala N, Sidis Y, DiTusa J F, Aeppli G, Young D and Fisk Z 2000 Magneto resistance from quantum interference effects in ferromagnets *Nature* **404** 581–4

Mattheiss L F and Hamann D R 1993 Band-structure and semiconducting properties of FeSi *Phys. Rev.* B **47** 13114–9

Menzel D, Popovich P, Kovaleva N N, Schoenes J, Doll K and Boris A V 2009 Electron–phonon interaction and spectral weight transfer in $Fe_{1-x}Co_xSi$ *Phys. Rev.* B **79** 165111

Nix F C and MacNair D 1941 The thermal expansion of pure metals: copper, gold, aluminum, nickel, and iron *Phys. Rev.* **60** 597–605

Park C-H, Shen Z X, Loeser A G, Dessau D S, Mandrus D G, Migliori A, Sarrao J and Fisk Z 1995 Direct observation of a narrow band near the gap edge of FeSi *Phys. Rev.* B **52** 981–4

Paschen S, Felder E, Chernikov M, Degiorgi L, Schwer H, Ott H, Young D, Sarrao J and Fisk Z 1997 Low-temperature transport, thermodynamic, and optical properties of FeSi *Phys. Rev.* B **56** 12916–30

Pauling L and Soldate A M 1948 The nature of the bonds in the iron silicide, FeSi, and related crystals *Acta Crystallogr.* **1** 212–6

Petrova A E, Krasnorussky V N, Yuhasz W M, Lograsso T A and Stishov S M 2011 Elastic properties of MnSi, FeSi and CoSi *J. Phys.: Conf. Ser.* **273** 12056

Poirier J-P 2000 Introduction to the physics of the earth's interior (Cambridge: Cambridge University Press)

Ross N L 1996 High-pressure single-crystal x-ray diffraction study of ϵ-FeSi *Acta Crystallogr.* A **52** C530

Sales B C, Delaire O, McGuire M A and May A F 2011 Thermoelectric properties of Co-, Ir-, and Os-doped FeSi alloys: evidence for strong electron–phonon coupling *Phys. Rev.* B **83** 1–7

Sales B C, Jones E C, Chakoumakos B C, Fernandez-Baca J A, Harmon H E, Sharp J W and Volckmann E H 1994 Magnetic, transport, and structural properties of $Fe_{1-x}Ir_xSi$ *Phys. Rev.* B **50** 8207–13

Samuely P, Szabó P, Mihalik M, Hudáková N and Menovsky A A 1996 Gap formation in Kondo insulator FeSi: point contact spectroscopy *Physica* B **218** 185–8

Sata N, Hirose K, Shen G, Nakajima Y, Ohishi Y and Hirao N 2010 Compression of FeSi, Fe_3C, $Fe_{0.95}O$, and FeS under the core pressures and implication for light element in the Earth's core *J. Geophys. Res.* **115** B09204

Schlesinger Z, Fisk Z, Zhang H T, Maple M B, DiTusa J and Aeppli G 1993 Unconventional charge gap formation in FeSi *Phys. Rev. Lett.* **71** 1748–51

Semenova E 2009 Iron–nickel–silicon Landolt-Börnstein - Group IV Physical Chemistry 11D5 (Ternary Alloy Systems) pp 238–58

Shi N, Bai W, Li G, Xiong M, Yang J, Ma Z and Rong H 2012 Naquite, FeSi, a new mineral species from Luobusha, Tibet, Western China *Acta Geol. Sin.* **86** 533–8

Toby B H 2001 EXPGUI, a graphical user interface for GSAS *J. Appl. Crystallogr.* **34** 210–3

Vočadlo L, Knight K S, Price G D and Wood I G 2002 Thermal expansion and crystal structure of FeSi between 4 and 1173 K determined by time-of-flight neutron powder diffraction *Phys. Chem. Miner.* **29** 132–9

Vočadlo L, Price G D and Wood I G 1999 Crystal structure, compressibility and possible phase transitions in epsilon-FeSi

studied by first-principles pseudopotential calculations *Acta Crystallogr.* B **55** 484–93
Vočadlo L, Price G D and Wood I G 2000 Structures and physical properties of 4-FeSi-type and CsCl-type RuSi studied by first-principles pseudopotential calculations research papers *Acta Crystallogr.* B **56** 369–76
Wallace D C 1998 *Thermodynamics of Crystals* (New York: Dover)
Whitaker M L, Liu W, Liu Q, Wang L and Li B 2009 Thermoelasticity of ε-FeSi to 8 GPa and 1273 K *Am. Mineral.* **94** 1039–44
Wood I G, Ahmed J, Dobson D P and Vočadlo L 2013 High-pressure phase transitions and equations of state in NiSi. III. A new high-pressure phase of NiSi *J. Appl. Crystallogr.* **46** 14–24
Wood I G, David W I F, Hull S and Price G D 1996 A high-pressure study of e-FeSi, between 0 and 8.5 GPa, by time-of-flight neutron powder diffraction *J. Appl. Crystallogr.* **29** 215–8
Yadam S, Singh D, Venkateshwarlu D, Gangrade M K, Samatham S S and Ganesan V 2016 Metal to insulator transition and an impurity band conduction in $Fe_{1-x}Cr_xSi$ *J. Alloys Compd.* **663** 311–5
Zhang W-W, Xu H, Liang J-L, Xiong W and Du Y 2009 Phase equilibria of the Fe–Ni–Si system at 850 °C *J. Alloys Compd.* **481** 509–14
Zinoveva G P, Andreeva L P and Geld P V 1974 Elastic constants and dynamics of crystal lattice in monosilicides with B20 structure *Phys. Status Solidi* A **23** 711–8